Catalysis Science & Technology

Accepted Manuscript

ROYAL SOCIETY OF CHEMISTRY

www.rsc.org/catalysis

Catalysis Science & Technology RSC

ARTICLE

Partial hydrogenation of acetylene over NiTi layered double hydroxide supported PdAg catalyst

Y. N. Liu [1], J. T. Feng [1,*], Y. F. He [1], J. H. Sun [2], D. Q. Li [1,*]

ABSTRACT: NiTi layered double hydroxide (NiTi-LDH) with rich defective sites was synthesized and used as the support for the preparation of a novel supported PdAg nanoalloys catalyst for the partial hydrogenation of acetylene. The obtained PdAg/NiTi-LDH catalyst exhibited a remarkable catalytic performance. When the conversion of acetylene reached 90%, the selectivity towards ethene maintained 82%. Superior hydrogenation activity was ascribed to two key factors. Small particle size and high dispersion of PdAg nanoparticles were responsible for boosting the catalytic activity. In addition, Ti^{3+} defective sites in the support also played an important role on the enhancement of activity. The interface at the Ti^{3+} species and active metals acting as new active sites enhanced the activation and dissociation of hydrogen and therefore further improved catalytic activity. Preferable selectivity was assigned to the electronic effect between NiTi-LDH support and PdAg nanoalloys. The electron transfer from the Ti^{3+} species to Pd resulted in the increase of electron density and the linearly coordinated sites of Pd and therefore facilitated the desorption of ethene. Moreover, due to the reducibility of NiTi-LDH, the selectivity and stability over reduced PdAg/NiTi-LDH catalyst were further enhanced on account of the strong metal-support interaction.

1. Introduction

Ethene is an important polymerization feedstock and intermediate in many industrial reactions. It is typically obtained by thermal or catalytic cracking of higher hydrocarbons. During this process, a small quantity of acetylene is produced inevitably. The trace of acetylene in the stream can poison the olefin polyethylene catalysts.[1-3] Therefore, the acetylene content in the feedstock has to be reduced to at least 5 ppm. Supported Pd catalyst is commercially used for this purpose, but shows poor selectivity and stability.[4, 5]

There are several approaches to improve selectivity at high acetylene conversion including the addition of a second metal and screen of a suitable support. The role of the second metal (e.g. Ag, Ni, Cu, Ga and Zn) in the Pd-based catalyst is generally considered to be derived from two factors: geometric effect and/or electronic effect.[6, 7] Among possible bimetallic Pd-based catalysts, PdAg catalyst has attracted extensive attention. Zhang et al.[8] found that bimetallic PdAg catalyst possessed higher selectivity because the introduction of Ag diluted the multiply coordinated sites of Pd and then enhanced the selectivity of ethene owing to the geometric effect. Neurock and co-workers[9] revealed that the addition of Ag into Pd catalyst could increase the electron density of the Pd d-band as a result of charge transfer from Ag to Pd, which weakened the adsorption of both ethene and acetylene on the alloy surface. Except for active components, the effect of support is also of importance for the partial hydrogenation of acetylene such as surface area, pore distribution and acid-base property of the support. Panpranot and co-workers [10] found that the mixed phases Al_2O_3 supported Pd catalysts with higher BET surface area resulted in significant improvements in both acetylene conversion and ethylene selectivity compared to that of γ-Al_2O_3 or α-Al_2O_3. Chen et al.[2] confirmed the novel and promising catalytic properties of zeolite supported bimetallic catalysts compared with those supported on γ -Al_2O_3 due to the multidimensional pore system with large pore apertures of zeolite. Moreover, some research groups reported that the catalyst support with rich defect sites could change the electronic properties of metals[11, 12] and consequently obtain preferable catalytic performance. Panpranot and co-workers[13] reported that Pd catalysts supported on TiO_2 with Ti^{3+} defects exhibited higher selectivity towards ethene in the partial hydrogenation of acetylene. The existence of Ti^{3+} defective sites increased the electron density of close-contacted Pd and weakened the adsorption strength of ethene. Therefore, developing a novel bimetallic PdAg alloy catalyst using possible materials with rich defect sites as supports for partial hydrogenation of acetylene could be remarkably valuable.

Layered double hydroxides (LDHs) are a class of typical 2D inorganic layered matrices with a general formula of $[M^{2+}_{1-x}M^{3+}_x(OH)_2]^{x+}(A^{n-})_{x/n}\cdot mH_2O$. The M^{2+} and M^{3+} cations are uniformly dispersed within the layers.[14] Owing to the flexibility in composition

and the special structure, LDHs have been a promising materials used as catalyst supports and actual catalysts.[15-18] Wei and co-workers[19] demonstrated that Ti-containing LDH displayed abundant surface defects served as trapping electrons which significantly enhanced photocatalytic activity compared to bulk Ti oxide. Liu and Hensen et al.[20] reported that the catalytic activity of Au catalysts for aerobic oxidation of alcohols can be significantly improved by using Cr-containing LDH as the support. The results showed that O_2 could be activated on Cr^{3+} defect sites in the surface layer, resulting in Cr^{6+} species and basic hydroxyl with electron transfer from Cr-LDH support to Au nanoparticles. However, the application and beneficial effect of using this specific material with rich defective sites as catalyst supports for partial hydrogenation are rarely reported. Therefore, the combination of bimetallic PdAg nanoalloys with rich defected LDH support as a novel heterogeneous catalyst for partial hydrogenation of acetylene is of great significance. In the present work, a novel supported PdAg nanoalloy catalyst for partial hydrogenation of acetylene was fabricated by using NiTi-LDH with rich defective sites as the support. The structural properties of the catalyst were characterized by XRD, XPS, ESR, HRTEM and N_2 adsorption-desorption. Special attention was paid to the relationship between surface properties of the catalyst and catalytic performance. Especially, the influence of surface defects as well as the interface between metal and support on metal particle size, the amount of active sites and electronic properties of metals were investigated. Furthermore, due to the reducibility of NiTi-LDH support, the obtained PdAg/NiTi-LDH catalyst was further reduced at high temperature to study the strong metal-support interaction (SMSI) effect.

2. Experimental

2.1 Materials

$Ni(NO_3)_2{\cdot}6H_2O$, $TiCl_4$, urea, $PdCl_2$, NaCl, $NaBH_4$, Poly vinyl alcohol and commercial TiO_2 were purchased from Aladdin Co.. Commercial $PdAg/Al_2O_3$ catalyst (BCH-20B, tooth spherical) were purchased from the Beijing Chemical Industry Research Institute. PVA (MW≈2000) and acetone (A.R. Grade) were obtained from Beijing Chemical Co. and used without further purification. The water used in all the experiments was deionized and had an electrical conductivity<10^{-6} $S{\cdot}cm^{-1}$.[18]

2.2 Preparation of NiTi-LDH support

0.5 mL of $TiCl_4$ solution (V_{TiCl4}:V_{HCl}=1:1, $TiCl_4$ is 0.002 mol), 0.01 mol of $Ni(NO_3)_2{\cdot}6H_2O$ and 0.1 mol of urea were dissolved in 100 mL deionized water under vigorous stirring for 10 h at reflux temperature (100 °C). The resulting solid was centrifuged, washed with deionized water, and dried at 60 °C.

2.3 Preparation of supported PdAg nanoalloy catalysts

Using the co-reduction method in the synthesis of PdAg alloy catalysts, $PdCl_2$ was employed as the Pd^{2+} precursor. Na_2PdCl_4 solution was prepared by dissolving 0.6440 g of $PdCl_2$ and 0.4250 g of NaCl in 100 mL of deionized water and stirred until it was completely dissolved. 560 μL of Na_2PdCl_4 solution and 400 μL of $AgNO_3$ solution (dissolving 0.8495 g of $AgNO_3$ in 100 mL of deionized water) together with 0.0080 g of $NaBH_4$ and 0.0052 g of PVA were mixed together under vigorous stirring. After stirring for 1 h at room temperature, dark grey PdAg colloidal solution was obtained. To prepare supported catalyst, 0.1440 g of NiTi-LDH was then added into PdAg colloidal solution and was stirred for another 1 h. The resulting suspension was centrifuged, washed with deionized water as well as anhydrous acetone, and dried at 60 °C. As comparison, commercial TiO_2 and the prepared $Ni(OH)_2$ supported PdAg alloy catalysts were also synthesized under the premise of remaining other conditions unchanged. Preparation method of $Ni(OH)_2$ was stated as follows: 2.9070 g of $Ni(NO_3)_2{\cdot}6H_2O$ and 6.5000 g of urea were dissolved in 100 mL deionized water under vigorous stirring for 10 h at reflux temperature (100 °C). The resulting solid was centrifuged, washed with deionized water and dried at 60 °C. To investigate the interaction between metal and support after high temperature reduction, PdAg/NiTi-LDH catalyst was further calcined at 500 °C in H_2 for 4 h before acetylene hydrogenation and the obtained catalyst was denoted as PdAg/NiTi-LDH-H_2-R.

2.4 Characterizations

XPS of the samples was collected using a Thermo VG ESCALAB 250 spectrometer equipped with Mg Kα anode. The calibration peak is the C 1s peak at 284.6 eV. X-ray diffraction (XRD) patterns were performed by a Shimadzu XRD-6000 diffractometer using Cu Kα source (λ= 0.154 nm) in the 2θ range from 3° to 70° and a scan step of 10° min^{-1}. The specific surface area was calculated according to the Brunauer-Emmett-Teller (BET) method based on the adsorption isotherm. The Barrett-Joyner-Halenda (BJH) method was used to calculate the pore volume and the pore size distribution. The lattice fringes of the catalysts were characterized using a JEOL JEM-2100 high-resolution transmission electron microscope (HRTEM). Chemical analyses were obtained with inductively coupled plasma emission spectroscopy (ICP-AES; a Shimadzu ICPS-75000). Electron spin resonance (ESR) spectroscopy was conducted under vacuum at -150 °C without illumination using a JEOL electron spin resonance spectrometer. It was performed to qualitatively and quantitatively monitor the Ti^{3+} species on the surface of the TiO_2 and NiTi-LDH.

Pulse CO chemisorption, temperature-programmed reduction (TPR) and C_2H_4-TPD were carried out using Micrometric Chemisorb 2750 chemisorption instrument with a thermal conductivity detector (TCD). The dispersion of the catalysts was determined by pulse carbon monoxide (CO) chemisorption. In general, pure Ag does not chemisorb CO and therefore CO chemisorption occurred only on Pd atoms on the surface of PdAg nanoalloys. A CO/Pd average stoichiometry of 1 has been assumed for calculation of the dispersion.[2] After pre-treatment, multiple pulses of a 5% CO/He mixture were passed over the catalyst from a 330 μL sample injector at room temperature until a constant CO peak area was observed. TPR was recorded using 10% H_2 in Ar with a total flow rate of 25 $mL{\cdot}min^{-1}$, heated from room temperature to 550 °C. Prior to C_2H_4-TPD, 0.1000 g catalysts were heated at 120 °C for 30 min in argon and cooled to room temperature. The catalyst was kept until the adsorption was saturated in a stream of ethene with helium as a carrier gas, then the catalyst was purged with helium for 30 min. C_2H_4-TPD was controlled by heating from room temperature to 450 °C. Prior to H_2-TPD, the catalysts were also heated at 120 °C for 2 h in nitrogen and then placed in 10 % H_2/Ar with a flow rate of 40 $mL{\cdot}min^{-1}$ for 0.5 h at 30 °C. TPD was carried out in a stream of argon with a flow rate of 40 $mL{\cdot}min^{-1}$ and a

temperature ramp of 10 °C min^{-1}. The experimental error in TPD temperatures is ±3 °C according to repeated tests. TPO analyses were also carried out on catalyst samples. After a time-on-stream hydrogenation process, the catalysts were transferred into a quartz reactor followed by heating in He flow for 60 min at 120 °C. The gas composition was then switched to 10% O_2 in helium, and the temperature was increased to 600 °C at a ramp rate of 10 °C min^{-1}.

2.5 Partial hydrogenation of acetylene

Acetylene hydrogenation was investigated in a Xian Quan WFS-3015 fixed bed microreactor over the temperature range from 30-90 °C with total flow rate of 167.5 mL min^{-1}, reaction pressure of 0.4 MPa, and a space velocity (GHSV) of 10050 h^{-1}, 33.2% C_2H_4/C_2H_2 mixed gases (containing 0.967% acetylene in ethene), 0.6% H_2, and 66.2% N_2 (H_2/C_2H_2=2). A 0.05 g of catalyst and 1.95 g (1.25 mL) of quartz sand were mixed and filled into the reactor. Prior to reaction, the samples were reduced in hydrogen at 100 °C for 1 h with a flow rate of 5 mL·min^{-1}. The reactants and products were analyzed by gas chromatography (GC) with a flame ionization detector online using a PLOT capillary column (0.530 m × 50 mm). Acetylene conversion and ethene selectivity are defined as follows: [8]

$$\text{Acetylene conversion} = \frac{C_2H_2\,(\text{inlet}) - C_2H_2\,(\text{outlet})}{C_2H_2\,(\text{inlet})}$$

$$\text{Ethene selectivity} = \frac{C_2H_4\,(\text{outlet}) - C_2H_4\,(\text{inlet})}{C_2H_2\,(\text{inlet}) - C_2H_2\,(\text{outlet})}$$

3. Results and discussion

3.1 Catalytic performance in partial hydrogenation of acetylene

The catalytic performance including activity and selectivity towards ethene of the NiTi-LDH with two kinds of transition metal supported PdAg catalyst for partial hydrogenation of acetylene in an ethene-rich stream was tested in a fixed-bed flow reactor. For comparison purposes, TiO_2 and $Ni(OH)_2$ supported PdAg catalysts were also tested under the employed reaction conditions. In this work, catalytic activity is defined as the rate of acetylene consumption, which is expressed as the moles of acetylene conversion in unit time. Therefore, higher acetylene conversion represents higher rate/activity.[21] The Pd loading and the Ag loading of the three catalysts, obtained from ICP analysis, were shown in table 2. The actual values were slightly different from the theoretical value (1.4%), but the values are allowable within experimental error. The result rules out the influence of different Pd and Ag content on the catalytic performance, indicating the activity related to the nature of the catalyst. Figure 1A shows plots of acetylene conversion versus reaction temperature over different catalysts. With the reaction temperature increasing, the acetylene conversion increases. The PdAg/NiTi-LDH catalyst exhibited much higher acetylene conversion than that of other PdAg catalysts with different supports. Especially, when the reaction temperature increased to 70 °C, the acetylene conversion of PdAg/NiTi-LDH catalysts reached 90% which was 30% and 60% higher than that of PdAg/TiO_2 and PdAg/$Ni(OH)_2$, respectively. To eliminate the contribution of NiTi-LDH support, catalytic performance of the pristine NiTi-LDH was also tested. As shown in Figure 1A, the acetylene conversion of NiTi-LDH was less than 5% ranging from 30 to 90 °C indicating that the contribution of NiTi-LDH support on the catalytic performance can be ignored. Selectivity at a fixed conversion for the catalysts is shown in Figure 1B. The selectivity toward ethene of the three catalysts decreased with conversion increasing and at iso-conversions selectivity toward ethene decreased in the order PdAg/NiTi-LDH> PdAg/TiO_2> PdAg/$Ni(OH)_2$. Compared with monometallic Pd catalyst reported in literatures,[21, 22] all of the three catalysts exhibited much higher selectivity towards ethene on account of the synergistic effect of bimetallic PdAg nanoalloys. When the conversion of acetylene reached 90%, ethene selectivity over PdAg/NiTi-LDH maintained 82%, which is remarkably higher than that over the reported catalysts as well as commercial PdAg/Al_2O_3 catalyst shown in Table 1.[21-26] The preferable catalytic performance of PdAg/NiTi-LDH catalyst might be attributed to the structural nature of the catalyst itself including large specific surface area, [10] high metal dispersion, [27, 28] enhanced interface effect[29, 30] and/or the change of electronic properties of metals.[11, 12]

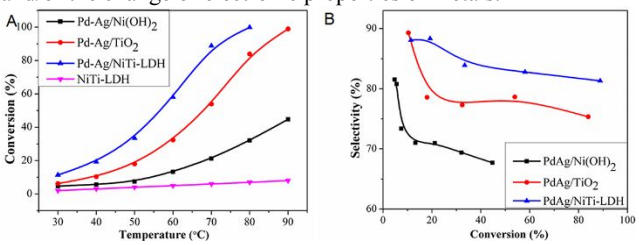

Fig. 1 Plots of (A) the acetylene conversion versus reaction temperature and (B) the ethene selectivity versus conversion at a total flow rate of 167.5 mL/min (GHSV: 10050 h^{-1}) with varying reaction temperature from 30 to 90 °C.

3.2 The study of structure-property relationship

3.2.1 Crystalline structure of the catalyst

To explore the crystal structure of the catalysts, XRD analysis of metallic colloidal sol (A) and the prepared NiTi-LDH, $Ni(OH)_2$ and commercial TiO_2 supports (B) were carried out and the patterns are shown in Figure 2. The pattern of the metallic colloidal sol showed two diffraction peaks that can be indexed to diffraction from the (111) and (200) of the face-centered cubic (fcc) structure of metallic PdAg. The diffraction peaks of bimetallic PdAg were coincidently located between Pd (JCPDS 46-1043) and Ag (JCPDS 04-0783), indicating the formation of PdAg nanoalloys.[8] The d_{111} and d_{200} of PdAg nanoalloys were calculated to be 0.230 nm and 0.197 nm according to Bragg formula. As shown in Figure 2B, the XRD pattern of NiTi-LDH (curve a) can be indexed as a rhombohedral structure with the typical (003), (006), (009) and (110) reflections at $2\theta \approx 12.2^{\circ}$, 24.5°, 33.5°, and 59.7° with a basal spacing (d_{003}) of 0.722 nm ($2\theta \approx 12.2^{\circ}$) illustrating that the interlayer anion is CO_3^{2-}.[19] No other crystalline phase was detected, which demonstrated the high purity of NiTi-LDH. The pattern of the prepared $Ni(OH)_2$ (curve b) exhibited strong diffraction peaks corresponding to diffraction from the (001), (100), (101), (102) and (110) suggesting the formation of $Ni(OH)_2$.[31] The pattern of the commercial TiO_2 support shown as curve c exhibited the characteristic reflections of (101), (004), (200), (105) and (204) indicating TiO_2 was in the anatase phase.[13] However, due to the low loading and the small particle size of PdAg nanoalloys, no obvious diffraction peaks can be observed

Catalysis Science & Technology RSC

ARTICLE

Table 1 Ethene selectivity at acetylene conversion 90% on various catalysts.

Catalysts	Ethene Selectivity (%)	Pd Loading (%)	GHSV (h^{-1})	H_2/C_2H_2	Reaction pressure (MPa)
PdAg/NiTi-LDH [a]	82	1.42	10050	2	0.4
PdAg/TiO_2 [a]	75	1.44	10050	2	0.4
Commercial PdAg/Al_2O_3 (BCH-20B) [a]	51	0.04	10050	2	0.4
Cuboc Pd/MgAl−LDH[21]	68	2.40	8040	2	0.4
Pd_5Ga/MgO-Al_2O_3[22]	81	5.00	10056	2	0.05
Pd/MgO-Al_2O_3[22]	50	5.00	10056	2	0.05
Flowerlike PdAu/MgAl-MMO[23]	70	1.00	1607-11255	2	0.2
Octahedra PdAu/MgAl-MMO[23]	56	1.00	1607-11255	2	0.2
PdAg/Al_2O_3(impregnation)[24]	20	1.00	4000-16 000	2	Not reported
PdCu/Al_2O_3(surface redox) [25]	38	1.00	3000-13500	2	Not reported
PdAg/Al_2O_3(surface redox) [25]	40	1.00	3000-13500	2	Not reported
Pd-Si/SiO_2 [26]	38	1.00	4000-16 000	2	Not reported
Pd/SiO_2[26]	25	1.00	4000-16 000	2	Not reported

[a] tested in this work

after immobilizing onto the support. Therefore, the XRD patterns of the supported catalysts were not given.

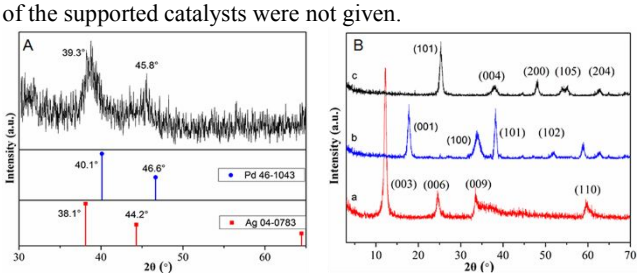

Fig. 2 XRD patterns of (A) the PdAg colloidal sol and (B) the supports: (a) the prepared NiTi-LDH, (b) $Ni(OH)_2$ and (c) commercial TiO_2

3.2.2 Textural properties of support and the catalysts

BET surface areas of the supports were listed in Table 2. The specific surface areas of NiTi-LDH and TiO_2 were significantly larger than that of $Ni(OH)_2$. In general, high surface area of the support could provide high dispersion of active metals, which facilitates the improvement of the catalytic activity.[32] This result was consistent with the trend of catalytic performance in figure 1. In addition, according to the literatures, high dispersion of active metals could also be ascribed to the strong metal−support interaction (SMSI). [33, 34] SMSI effect of the PdAg/NiTi-LDH catalyst will be confirmed in the following discussion. HRTEM images and the corresponding size distribution of PdAg nanoparticles on different supports are shown in Figure 3. As expected, PdAg nanoparticles dispersed more homogeneously on the surface of NiTi-LDH and TiO_2 compared with those on $Ni(OH)_2$. To measure the distribution and mean size, 200 particles in different regions were randomly selected. The mean size of the PdAg nanoparticles in PdAg/NiTi-LDH, PdAg/TiO_2 and PdAg/$Ni(OH)_2$ is 2.6 nm, 3.1 nm and 5.6 nm, respectively. Moreover, the lattice spacing of the metallic colloidal sol was measured to be 0.230 nm and 0.197 nm corresponding to the (111) and (100) facets of PdAg nanoalloy and were well consistent with XRD results, further indicating the formation of PdAg alloy. The dispersion of supported PdAg catalysts was determined by CO chemisorption experiments[35] and the corresponding values were listed in Table 1. It is obviously observed that the dispersion of PdAg supported on NiTi-LDH is 15% and 40% higher than that of PdAg supported on TiO_2 and $Ni(OH)_2$ which was consistent with the trend calculated by the particle size from HRTEM images. In general, nanoparticles possessed narrower distribution, smaller particle size and higher dispersion could increase the proportion of active metal surface atoms to bulk phase atoms, and thus improve the catalytic performance.[26] Therefore, smaller particle size and higher dispersion of PdAg/NiTi-LDH could be the contribution on the preferable catalytic performance compared with that of PdAg/TiO_2 and PdAg/$Ni(OH)_2$. However, this difference in the particle size and dispersion of PdAg particles can not considered to be the only reason for the disparity in the catalytic activity observed for PdAg/TiO_2 and PdAg/NiTi-LDH. As a result, we will further explore the other factors for the difference of catalytic activity of PdAg/TiO_2 and PdAg/NiTi-LDH.

Catalysis Science & Technology RSC

ARTICLE

Table 2 Textural properties of support and the catalysts.

Samples	BET surface area [a] ($m^2 \cdot g^{-1}$)	Pd Loading[b] (%)	Ag loading[b] (%)	Pd dispersion[c] (%)	$\bar{d}_{fresh}$-Pd[d] (nm)
NiTi-LDH	104.27	-	-	-	-
TiO_2	101.99	-	-	-	-
$Ni(OH)_2$	48.88	-	-	-	-
PdAg/NiTi-LDH	-	1.42	1.11	31.5	2.6
PdAg/TiO_2	-	1.44	1.10	25.8	3.0
PdAg/$Ni(OH)_2$	-	1.43	1.11	11.2	5.6

[a] Determined by BET analysis; [b] Determined by ICP analysis; [c] Determined by CO-chemisorption; [d] Determined by HRTEM.

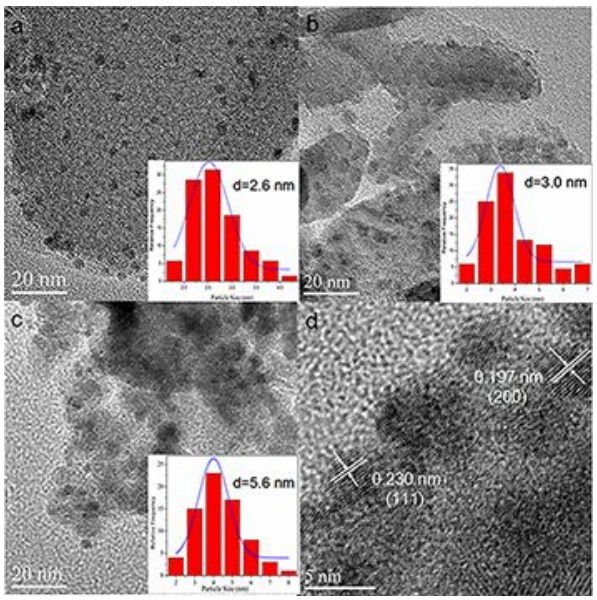

Fig. 3 HRTEM images of (a) PdAg/NiTi-LDH, (b) PdAg/TiO_2 and (c) PdAg/$Ni(OH)_2$ (d) PdAg colloidal sol. Inset in the corresponding images show the particle size frequency distribution histograms.

3.2.3 Characterizations of defects in the supports

It is reported that NiTi-LDH and TiO_2 supports contain surface defect (Ti^{3+}) which are produced by trapping of electrons and the amount of accumulated electrons may reflect the number of defect sites.[36] Based on the catalytic results, the PdAg nanoparticles supported on NiTi-LDH and TiO_2 with Ti^{3+} defective sites exhibited much higher activity than those on $Ni(OH)_2$ support which suggested the existence of Ti^{3+} defects may facilitate the catalytic performance. In order to qualitatively investigate the Ti^{3+} defects containing in the supports, electron spin resonance (ESR) technology was performed over both NiTi-LDH and anatase TiO_2 supports and the results are shown in Figure 4. Nakaoka and Nosaka[37] reported six signals of ESR measurement occurring on the surface of titania: (i) $Ti^{4+}O^{-}Ti^{4+}OH^{-}$, (ii) surface Ti^{3+}, (iii) adsorbed oxygen (O^{2-}), (iv) $Ti^{4+}O^{2-}Ti^{4+}O^{2-}$, (v) inner Ti^{3+}, and (vi) adsorbed water. In this study, only one major signal at g values of 1.996 (less than 2) was observed in both NiTi-LDH and TiO_2 which can be assigned to Ti^{3+} (3d1) at the surface.[38] Furthermore, the intensity of the Ti^{3+} signal of the co-precipitation derived NiTi-LDH was higher than the commercial TiO_2, suggesting larger amount of defects in NiTi-LDH.

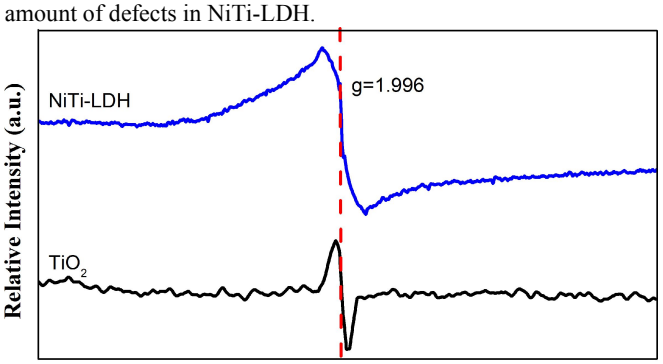

Fig. 4 ESR spectra of NiTi-LDH and TiO_2

To further quantitatively investigate the Ti^{3+} defects in two kinds of Ti containing materials, XPS analysis was performed. Ti $2p_{3/2}$ spectra of PdAg/NiTi-LDH and PdAg/TiO_2 were shown in Figure 5A. The XPS spectra of both PdAg/NiTi-LDH and PdAg/TiO_2 catalysts showed two peaks. After fitting, the peaks centered at 458.5 and 460.5 eV can be assigned to Ti^{4+}, which is consistent with the values reported in the literature, [13, 39] whereas the peak at

the lower binding energy of 456.7 and 458.9 eV can be attributed to Ti^{3+}. It is observed that the peak area ratio of Ti^{3+} to Ti^{4+} in PdAg/NiTi-LDH and PdAg/TiO_2 catalysts were obviously different. The Ti^{3+}/Ti^{4+} ratio of PdAg/NiTi-LDH catalyst is 0.47 which is much higher than that of PdAg/TiO_2 catalyst (0.22), indicating larger number of defects in the support of NiTi-LDH,[39] which is in accordance with the ESR results.

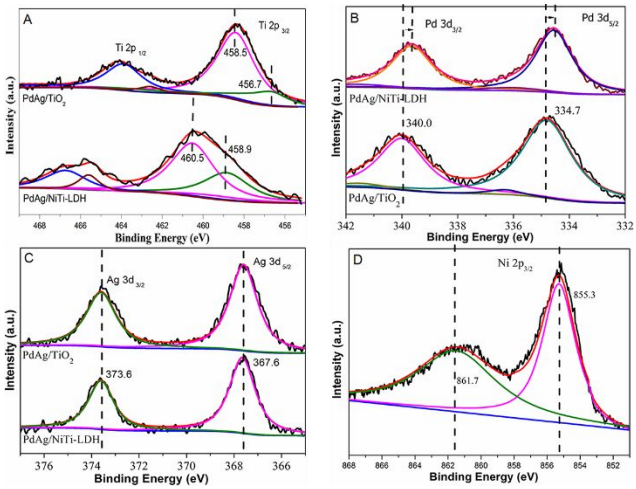

Fig. 5 Ti 2p (A), Pd 3d (B), Ag 3d (C) XPS spectra of PdAg/TiO_2, PdAg/NiTi-LDH catalysts and Ni 2p (D) XPS spectra of PdAg/NiTi-LDH catalyst.

3.2.4 H_2 dissociation/activation of the catalysts

Based on the previous report in the literature, we speculate that the interface of Ti^{3+} species in contact with palladium surface could act as new active sites which could more significantly enhance the activation and dissociation of hydrogen.[40] To gain information about H_2 activation/dissociation, H_2-TPD experiments were carried out on the PdAg/NiTi-LDH and PdAg/TiO_2 catalysts and the results are shown in Figure 6. Both catalysts showed at least two domain peaks of desorbed H_2, suggesting that hydrogen may be bounded to Pd surfaces with more than two adsorption states. The high temperature peak between 150~200 °C is attributed to the desorption of chemisorbed hydrogen, while the peak below 100 °C is attributed to the physically adsorbed hydrogen, which are more weakly bonded to the surface.[41, 42] As for PdAg/NiTi-LDH, the intensity of the desorption peak of chemisorbed hydrogen increased and the peak position remarkably moved to lower temperature compared with PdAg/TiO_2, indicating that H_2 dissociation/activation occurred more easily on the catalyst of PdAg/NiTi-LDH.

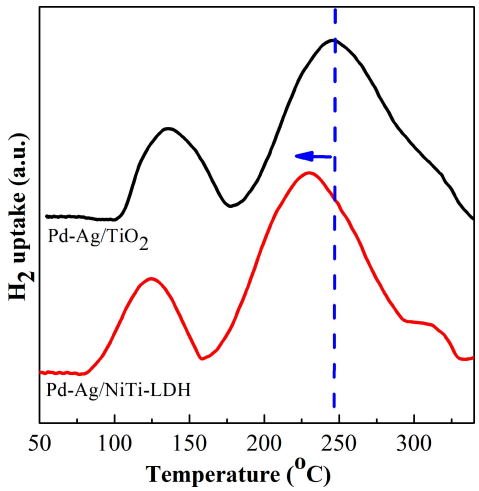

Fig. 6 H_2-TPD of PdAg/NiTi-LDH and PdAg/TiO_2 catalyst.

3.2.5 Electronic effect of the catalysts

To clarify the effect of Ti^{3+} defect sites on the interaction between PdAg nanoalloys and supports, XPS analysis was carried out and the results are shown in Figure 5. The XPS curves of Pd 3d (Figure 5B) were well fitted to two peaks. The one at lower binding energy (BE) is assigned to the electron transitions of Pd $3d_{5/2}$ and the higher one presents the electron transitions of Pd $3d_{3/2}$. The absence of characteristic peaks corresponding to Pd^{2+} indicates that all the Pd^{2+} precursor has been reduced to Pd^0. In comparison with the spectrum of PdAg/Al_2O_3,[8,43] the peak of Pd $3d_{5/2}$ over PdAg/TiO_2 and PdAg/NiTi-LDH catalysts were shifted to lower binding energy by approximately 0.3 eV and 0.5 eV, respectively. However, the Ti $2p_{3/2}$ and Ti $2p_{1/2}$ peaks assigned to the Ti^{3+} of PdAg/TiO_2 and PdAg/NiTi-LDH catalysts were slightly shifted to higher binding energies by about 0.2 eV and 0.4 eV compared with the pristine supports as shown in Figure 5A. For Ag $3d_{5/2}$, no obvious shift can be observed compared with the values in the literature [8, 43], as shown in Figure 5(C). The BE values of Ti^{4+} in Ti 2p spectra of PdAg/TiO_2 and PdAg/NiTi-LDH catalysts at around 358.5 and 360.5 eV are also in accordance with the reported values for the corresponding TiO_2 and NiTi-LDH.[13,39] Similarly, the XPS spectrum of PdAg/NiTi-LDH within the region of Ni $2p_{3/2}$ (Figure 5D) contained two peaks, appearing at binding energies around 855.3 and 861.7 eV which are corresponding to the characteristic peaks of Ni^{2+} and the shakeup satellite peak, respectively, which were well consistent with the values of pristine Ni-containing LDH reported in the literature.[44] The above results indicated that there was no obvious interaction between PdAg nanoalloys and Ni species or Ti^{4+} species, while there was the electron transition from the Ti^{3+} species to Pd resulting in the increase of electron density and the linearly coordinated sites of Pd and therefore easy desorption of ethene.[45-47] Especially, the higher degree of shift in PdAg/NiTi-LDH catalyst indicates much stronger metal-support interaction which leads to preferable ethene selectivity.

To further confirm the speculation based on XPS results, temperature programmed desorption (TPD) of ethene was performed to investigate the desorption capacity of ethene from the surface of PdAg/TiO_2 and PdAg/NiTi-LDH catalysts and the corresponding curves are shown in Figure 7. PdAg/TiO_2 shows two

major peaks. The one at the lower temperature (165 °C) is assigned to low-coordinated adsorbed ethene species, which were more weakly adsorbed and desorbed followed by the recombination of the surface hydrocarbon species to produce either ethene or ethane. The peak at ca. 235 °C is due to multi-coordinated adsorbed ethene species, which were easier to produce byproducts such as ethane.[47] In the case of PdAg/NiTi-LDH, three main desorption peaks were observed, among which the peak at ca. 330 °C was ascribed to the removal of CO_3^{2-} from the interlayer of NiTi-LDH.[47] The peak position related with the desorption of low-coordinated adsorbed ethene species moved to lower temperature by approximately 10 °C compared with that of PdAg/TiO_2, suggesting that ethene species were more easily desorbed from the surface of PdAg/NiTi-LDH catalyst, which is consistent with the speculation of XPS results.

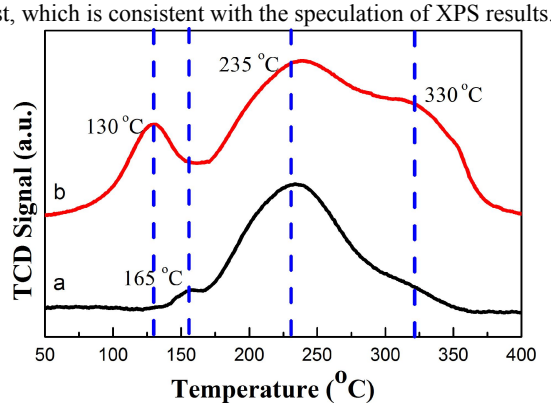

Fig. 7 Ethene-TPD from sample catalysts: (a) PdAg/TiO_2 and (b) PdAg/NiTi-LDH.

3.2.6 Possible mechanism of PdAg/NiTi-LDH catalyst

In summary, superior hydrogenation activity was ascribed to two main factors. Smaller particle size and higher dispersion of PdAg nanoparticles were responsible for the enhancement of catalytic activity. In addition, Ti^{3+} defective sites in the support also played an important role on improving the activity. The interface at the Ti^{3+} species and active metals acting as new active sites enhanced the activation and dissociation of hydrogen and therefore further improved catalytic activity. Preferable selectivity was assigned to the electronic effect between NiTi-LDH support and PdAg nanoalloys. The electron transfer from the Ti^{3+} species to Pd resulted in the increase of electron density and the linearly coordinated sites of Pd and therefore facilitated the desorption of ethene. The proposed mechanism for acetylene hydrogenation over PdAg/NiTi-LDH catalysts is illustrated in a conceptual model in Figure 8. The model shows two types of active sites. One of which created on the surface of Pd atoms; the other generated on the interface over Ti^{3+} species in contact with palladium surface which could more significantly enhance the activation and dissociation of hydrogen and therefore further enhance the activity. In addition, because of the elecronic effect between NiTi-LDH support and PdAg metals, the active sites were responsible for selective hydrogenation of acetylene to ethene and thus exhibited high ethene selectivity.

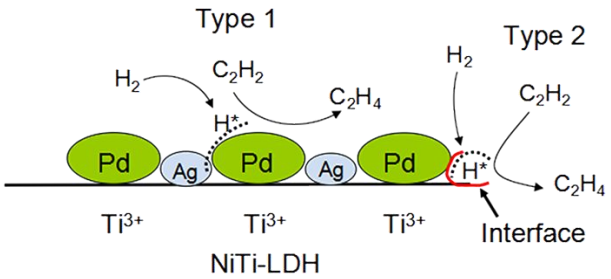

Fig. 8 Conceptual model for selective acetylene hydrogenation mechanism on PdAg/NiTi-LDH catalyst.

3.3 SMSI effect of the reduced PdAg catalysts

It is well known that the improvement of metal/support interactions could also lead to an enhanced selectivity in the partial hydrogenation reactions.[45-47] As reported, reducible metal oxides reduced at high temperature could migrate onto metallic surface, which enriches the electron density of the metals and increases the linearly coordinated sites of the metals and therefore weakens the ethene adsorption to improve ethene selectivity. This phenomenon is in the scope of the well-known strong metal-support interactions (SMSI) as demonstrated in previous works.[47]

TPR experiments were carried out to investigate the reducibility of the NiTi-LDH materials. Figure 9 presents the reduction profiles of NiTi-LDH and their corresponding supported PdAg catalysts. The maximum on the TPR curve of NiTi-LDH at about 398 °C can be related to the reduction of Ni species, the peak at about 357 °C can be interpreted as corresponding to the reduction of Ti species.[48, 49] The one at the 330 °C was ascribed to the removal of CO_3^{2-} from the interlayer of NiTi-LDH.[47] With the introduction of PdAg, the reduction peak relating to Ni species of the PdAg/NiTi-LDH catalyst shifted dramatically from 398 to 207 °C and the Ti species reduction peak also shifted to lower temperatures from 357 to 274 °C. These results clearly demonstrate that the presence of PdAg nanoparticles strongly promotes the reduction of NiTi-LDH and such promotion effect has been attributed to hydrogen activated on the metal phase induced by intimate metal-support interactions.[50] In addition, 500 °C was selected to further reduce the PdAg/NiTi-LDH in our work to study the SMSI effect.

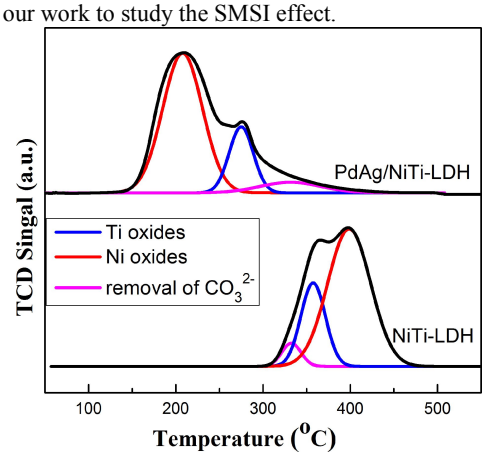

Fig. 9 TPR profiles for NiTi-LDH and PdAg/NiTi-LDH

Before acetylene hydrogenation reaction, PdAg/NiTi-LDH catalyst was calcined at 500 °C in H_2 for 4 h. Figure 10 shows plots of acetylene conversion versus reaction temperature (A) and plots

of ethene selectivity versus acetylene conversion (B) over PdAg/NiTi-LDH catalyst before and after reduction. The acetylene conversion of PdAg/NiTi-LDH-H_2-R catalyst is quite similar with the unreduced catalyst indicating the stability of PdAg/NiTi-LDH after high temperature reduction. The ethene selectivity increased by 5% after reduction, which might be attributed to the modification of the electronic structure of the Pd surface by partially reduced Ti and Ni oxides.[51] Furthermore, Ti^{3+} defective sites could easily diffuse from the lattice to surface of Pd particles to generate SMSI effect and therefore further enhance the selectivity.[51]

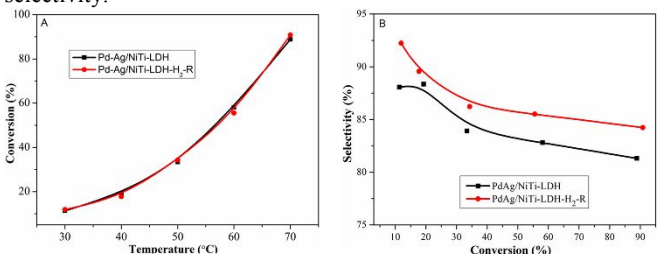

Fig. 10 Plots of the acetylene conversion (A) and ethene selectivity versus conversion (B) at a total flow rate of 167.5 mL/min (GHSV: 10050 h^{-1}) for PdAg/NiTi-LDH and PdAg/NiTi-LDH-H_2-R catalyst

To determine the influence of high temperature reduction on the electronic structure of catalysts, the XPS spectra of Ni 2p, Ti 2p and Pd 3d of PdAg/NiTi-LDH-H_2-R catalyst are shown in Figure 11. There are three peaks near 851.3 eV, 855.3 eV and 861.5 eV within the region of Ni $2p_{3/2}$ (Figure 11A), which are corresponding to the characteristic peaks of Ni^0, Ni^{2+} and the shake-up peak of Ni^{2+}, respectively.[52] The XPS spectrum of PdAg/NiTi-LDH-H_2-R within the region of Ti $2p_{3/2}$ (Figure 11B) contained three peaks, appearing at binding energies around 456.2, 458.4 and 460.0 eV, which were ascribed to Ti^{4+}, Ti^{3+}, Ti^{2+} species.[53] The results show that a part of Ni and Ti species containing in NiTi-LDH were reduced to Ni^0 and TiO_x. As shown in Figure 11C, the binding energy of Pd 3d shifted to a lower binding energy by approximately 0.2 eV compared with the unreduced catalyst (Figure 5C), which may indicate the charge transfer from the generated Ni^0 and TiO_x species to Pd. The charge transfer increases the electron density of Pd which facilitates desorption of ethene and therefore leads to preferable selectivity.

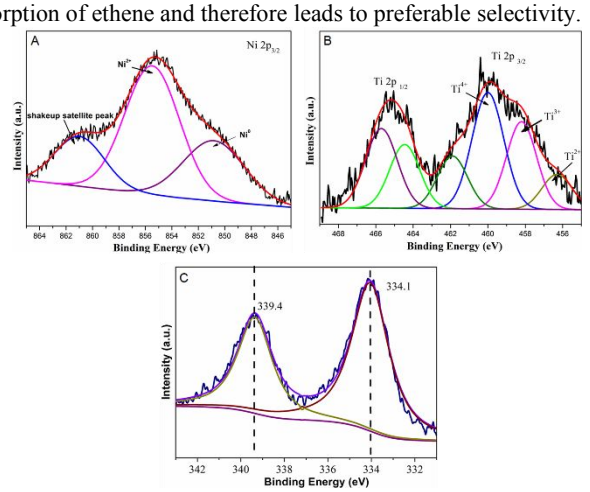

Fig. 11 Ni 2p (A), Ti 2p (B) and Pd 3d (C) XPS spectra of PdAg/NiTi-LDH-H_2-R catalysts

To investigate the stability of PdAg/NiTi-LDH and PdAg/NiTi-LDH-H_2-R catalysts, time-on-stream analysis was carried out at 70 °C with the relative pressure of 0.4 MPa for up to 48 h and the results are shown in Figure 12, in which t_0 represents the time when the reaction stabilized at this temperature. Unreduced PdAg/NiTi-LDH catalyst exhibited a pronounced deactivation behavior with time-on-stream increasing while the activity over the reduced PdAg/NiTi-LDH-H_2-R catalyst maintained an almost stable state in every test point during 48 h. This stable activity can be ascribed to two key factors, one of which was excellent resistibility against carbon deposition which partly suppress the block of active sites and therefore possessing preferable stability; [54] the other was structural stability of PdAg nanoalloys attributing to the existence of the strong interaction between PdAg nanoalloys and supports.

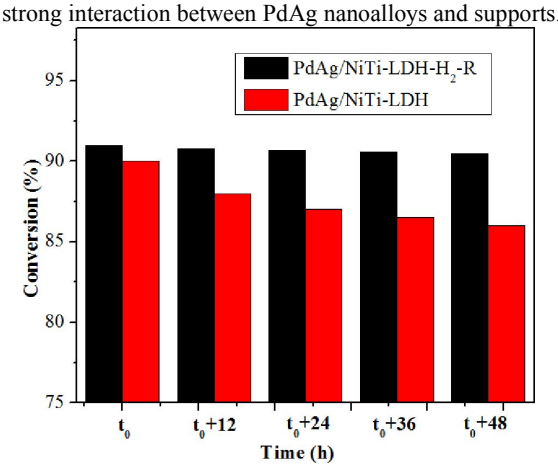

Fig. 12 Histogram of acetylene conversion versus reaction time over the PdAg/NiTi-LDH and PdAg/NiTi-LDH-H_2-R catalysts. (total flow rate: 167.5 mL/min (GHSV: 10050 h^{-1}) at reaction temperature 70 °C).

To obtain information about the formation of the carbonaceous deposits on the catalyst surface during the aging experiment, TPO analysis was conducted. Figure 13 presents the catalyst profile after the 48 h usage. The TPO profile indicated two peaks centered at 230 °C that can be ascribed to the combustion of coke associated to metal sites which can be considered to be harmless to the reaction, and the peak located around 350 °C can be associated with the combustion of amorphous coke, a precursor of graphitic carbon that has a structure of oligomeric hydrocarbon, C_xH_y, which reduces the availability of hydrogen and/or acetylene.[55-57] It can be easily figured out that the high temperature peak area of PdAg/NiTi-LDH-H_2-R catalyst was significantly smaller than that of PdAg/NiTi-LDH, indicating preferable resistance against carbonaceous compounds deposition and therefore possessing superior stability.

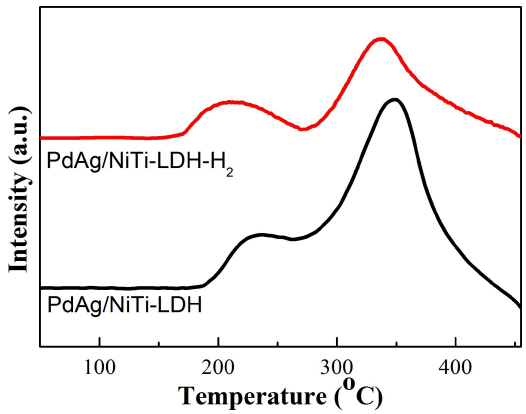

Fig. 13 TPO profiles of PdAg/NiTi-LDH and PdAg/NiTi-LDH-H_2-R catalysts after 48 h usage.

Besides of the resistance against carbon, structure stability of PdAg/NiTi-LDH-H_2-R catalyst is another important measurement towards stability of catalytic performance. HRTEM images of the two catalysts after continuous reaction for 48 h are shown in Figure 14. An increase in the mean size of PdAg nanoalloys was observed in the unreduced PdAg/NiTi-LDH catalyst from 2.6 to 3.4 nm due to the weak interaction between supports and active components. However, no obvious aggregation of PdAg nanoalloys was observed in the used PdAg/NiTi-LDH-H_2-R catalyst, indicating that the SMSI effect after high temperature reduction effectively suppress the migration and aggregation of PdAg nanoalloys and thus maintained preferable stability. Therefore, the favorable stability of PdAg/NiTi-LDH-H_2-R catalyst might be ascribed mainly to the excellent resistance against carbonaceous deposits and stability of the small PdAg nanoparticles size.

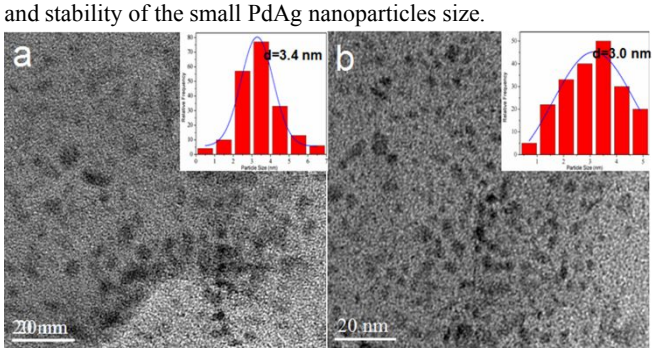

Fig. 14 HRTEM images of the used catalysts: (a) PdAg/NiTi-LDH and (b) PdAg/NiTi-LDH-H_2-R; Inset in the corresponding images show the particle size frequency distribution histograms.

4. Conclusion

A novel supported PdAg nanoalloy catalyst was designed and synthesized by using NiTi-LDH with rich defective sites as the support for the partial hydrogenation of acetylene. The obtained PdAg/NiTi-LDH catalyst exhibited much higher activity and selectivity compared with TiO_2 and $Ni(OH)_2$ supported PdAg catalysts. When the conversion of acetylene reached 90%, ethene selectivity over PdAg/NiTi-LDH catalyst maintained 82%. The excellent activity was ascribed to two key factors. The results of BET, HRTEM and CO chemisorption showed that the PdAg nanoparticles with smaller size and higher dispersion were found to boost catalytic activity. In addition, Ti^{3+} defective sites also play an important role on the enhancement of the catalytic performance. ESR and XPS results confirmed the existence of Ti^{3+} defective sites containing in the NiTi-LDH support and the number of Ti^{3+} defective sites was higher than that of commercial TiO_2. The interface at the Ti^{3+} species and active metals could act as new active sites which further enhanced the activation and dissociation of hydrogen confirmed by H_2-TPD. The preferable selectivity was assigned to the electronic effect between NiTi-LDH support and PdAg nanoalloys. XPS of the catalyst revealed the electron transfer from the Ti^{3+} species to Pd which resulted in the increase of electron density and the linearly coordinated sites of Pd and therefore facilitated the desorption of ethene affirmed by C_2H_4-TPD. Moreover, the SMSI effect between the metal and support was revealed by reducing the PdAg/NiTi-LDH catalyst at 500 °C. TPR analysis indicates that the NiTi-LDH is more likely to be reduced under the existence of PdAg nanoparticles. The reduced PdAg/NiTi-LDH catalyst exhibited much higher selectivity compared with the unreduced PdAg/NiTi-LDH catalyst. The SMSI effects in which Pd atoms draw electron density away from Ti^{3+} species enhanced the interaction of Pd atoms with the supports, and thereby increased the catalytic selectivity. In addition, the reduced catalyst exhibited preferable stability. One of the reasons was excellent resistibility against carbon deposition which partly suppress the block of active sites; the other was structural stability of PdAg nanoalloys attributing to the existence of the strong interaction between PdAg nanoalloys and supports. Consequently, the reduced PdAg/NiTi-LDH catalyst with simultaneously enhanced activity, selectivity and stability are of tremendous importance in the partial hydrogenation of acetylene.

Acknowledgements

This work was supported by the National Natural Science Foundation, the Support Plan Project (2012BAE06B08), 973 Project (2011CBA00506), Beijing Natural Science Foundation (2132032), Beijing Engineering Center for Hierarchical Catalysts, the Dean Project of Guangxi Key Laboratory of Petrochemical Resource Processing and Process Intensification Technology and the Doctoral Program of the Ministry of Education.

Notes and references

[1] *State Key Laboratory of Chemical Resource Engineering, Beijing University of Chemical Technology*
Address: *Box 98, 15 Bei San Huan East Road, Beijing 100029, China*
[2] *Guangxi Key Laboratory of Petrochemical Resource Processing and Process Intensification Technology, Guangxi University, Nanning 530004, China*
E-mail address:
lidq@mail.buct.edu.cn *(D. Q. Li);*
fengjt@mail.buct.edu.cn *(J. T. Feng)*

1 J. H. Kang, E. W. Shin, W. J. Kim, J. D. Park and S. H. Moon, *Catal. Today*, 2000, **63**, 183.
2 W. Huang, J. R. McCormick, R. F. Lobo and J. G. G. Chen, *J. Catal.*, 2007, **246**, 40.
3 P. Praserthdam, S. Phatanasri and J. Meksikarin, *Catal. Today*, 2000, **63**, 209.
4 G. C. Bond and P. B. Wells, *J. Catal.*, 1965, **5**, 65.
5 N. Wongwaranon, O. Mekasuwandumrong, P. Praserthdama and J. Panpranot, *Catal. Today*, 2008, **131**, 553.

6 D. C. Huang, K. H. Chang, W. F. Pong, P. K. Tseng, K. J. Hung and W. F. Hung, *Catal. Lett.* , 1998, **53**, 155.
7 E. W. Shin, C. H. Choi, K. S. Chang, Y. H. Na and S. H. Moon, *Catal. Today*, 1998, **44**, 137.
8 Q. W. Zhang, J. Li, X. X. Liu and Q. M. Zhu, *Appl. Catal. A: Gen.*, 2000, **197**, 221.
9 D. H. Mei, M. Neurock and C. M. Smith, *J. Catal.*, 2009, **268**, 181.
10 S. Komhoma, O. Mekasuwandumrong, P. Praserthdam and J. Panpranot, *Catal. Commun.*, 2008, **10**, 86.
11 L. N. Chen, X. Z. Wub, W. R. Huang, S. S. Mab and H. Xub, *Solid State Commun.*, 2012, **152**, 868.
12 Y. P. G. Chua, G. T. K. K. Gunasooriya, M. Saeys and E. G. Seebauer, *J. Catal.*, 2014, **311**, 306.
13 J. Panpranot, K. Kontapakdee and P. Praserthdam, *J. Phys. Chem. B.*, 2006, **110**, 8019.
14 X. X. Guo, F. Z. Zhang, D. G. Evans and X. Duan, *Chem. Commun.*, 2010, **46**, 5197.
15 C. Yu and J. He, *Chem. Commun.*, 2012, **48**, 4933.
16 M. Q. Zhao, Q. Zhang, W. Zhang, J. Q. Huang, Y. Zhang, D. S. Su and F. Wei, *J. Am. Chem. Soc.*, 2010, **132**, 14739.
17 Q. Wang and D. O'Hare, *Chem. Rev.*, 2012, **112**, 4124.
18 C. Roland-Swanson, J. Besse and F. Leroux, *Chem. Mater.*, 2004, **16**, 5512.
19 Y. F. Zhao, P. Y. Chen, B. S. Zhang, D. S. Su, S. T. Zhang, L. Tian, J. Lu, Z. X. Li, X. Z. Cao, B. Y. Wang, M. Wei, D. G. Evans and X. Duan, *Chem. Eur. J.*, 2012, **18**, 11949.
20 P. Liu, V. Degirmenci and E. J.M. Hensen, *J. Catal.*, 2014, **313**, 80.
21 Y. F. He, J. T. Feng, Y. Y. Du and D. Q. Li, ACS Catal., *ACS Catal.*, 2012, **2**, 1703.
22 Y. F. He, L. L. Liang, Y. N. Liu, J. T. Feng, C. Ma and D. Q. Li, *J. Catal.*, 2014, **309**, 166.
23 C. Ma, Y. Y. Du, J. T. Feng, X. Z. Cao, J. Yang and D. Q. Li, J. Catal., 2014, 317, 263.
24 J. H. Lee, S. K. Kim, I. Y. Ahn, W. J. Kim and S. H. Moon, *Catal. Commun.* , 2011, **12**, 1251.
25 S. K. Kim, J. H. Lee, I. Y. Ahn, W. J. Kim and S. H. Moon, *Appl. Catal. A: Gen.*, 2011, **401**, 12.
26 E. W. Shin, J. K. Kang, W. J. Kim, J. D. Park and S. H. Moon, *Appl. Catal. A: Gen.*, 2002, **223**, 161.
27 A. Sárkány, Z. Schay, K. Frey, é. Széles and I. Sajó, *Appl. Catal. A: Gen.*, 2010, **380**, 133.
28 W. G. Menezes, L. Altmann, V. Zielasek, K. Thiel and M. Bäumer, *J. Catal.*, 2013, **300**, 125.
29 S. Aranifard, S. C. Ammal and A. Heyden, *J. Catal.,* 2014, **309**, 314.
30 L. Bonneviot and G. L. Haller, *J. Catal.*, 1988, **113**, 96.
31 L. X. Yang, Y. J. Zhu, H. Tong, Z. H. Liang and W. W. Wang, *Cryst. Growth. Des.* , 2007, **7**, 2716.
32 M. J. Vincent and R. D. Gonzalez, *Appl. Catal. A: Gen.*, 2001, **217**, 143.
33 A. Douidah, P. Marécot, S. Szabo, J. Barbier, *Appl. Catal. A: Gen.*, 2002, **225**, 21.
34 H. A. E. Dole, L. F. Safady, S. Ntais, M. Couillard, E.A. Baranova, *J. Catal.,* 2014, **318**, 85.
35 W. Huang, W. Pyrz, R. F. Lobo and J. G. G. Chen, *Appl. Catal. A: Gen.*, 2007, **333**, 254.
36 S. Ikeda, N. Sugiyama, S. Murakami, H. Kominami, H. N. Y. Kera, K. Uosaki, T. Torimoto and B. Ohtani, *Phys. Chem. Chem. Phys.*, 2003, **5**, 778.
37 Y. Nakaoka and Y. Nosaka, *Photochem. Photobiol. A*, 1997, **110**, 299.
38 J. Panpranot, K. Kontapakdee and P. Praserthdam, *Appl. Catal. A: Gen.*, 2006, **314**, 128.
39 Y. F. Zhao, B. Li, Q. Wang, W. Gao, C. J. Wang, M. Wei, D. G. Evans, X. Duan and D. O'Hare, *Chem. Sci.*, 2014, **5**, 951.
40 P. Panagiotopoulou and D. I. Kondarides, *J. Catal.*, 2009, **267**, 57.
41 N. A. Khan, S. Shaikhutdinov and H. J. Freund, *Catal. Lett.* , 2006, **108**, 159.
42 W. Yu, G. M. Mullen and C. B. Mullins, *J. Phys. Chem. C.*, 2013, **117**, 19535.
43 R. N. Lamb, B. Ngamsom, D. L. Trimm, B. Gong, P. L. Silveston and P. Praserthdam, *Appl. Catal. A: Gen.*, 2004, **268**, 43.
44 J. T. Feng, Y. J. Lin, D. G. Evans, X. Duan and D. Q. Li, *J. Catal.*, 2009, **266**, 351.
45 W. J. Kim, I. Y. Ahn, J. H. Lee, S. H. Moon, *Catal. Commun.* , 2012, **24**, 52.
46 W. J. Kim and S. H. Moon, *Catal. Today*, 2012, **185**, 2.
47 E. Kim, E. W. Shin, C. W. Bark, I. Chang, W. J. Yoo and W. J. Kim, *Appl. Catal. A: Gen.*, 2014, **471**, 80.
48 Y. Wu, D. S. Wang, P. Zhao, Z. Q. Niu, Q. Peng and Y. D. Li, *Inorg. Chem.*, 2011, **50**, 2046.
49 C. A. González, M. Bartoszek, A. Martin and C. M. D.Correa, *Ind. Eng. Chem. Res.*, 2009, **48**, 2826.
50 L. Ma, D. S. Wang, J. H. Li, B. Y. Bai, L. X. Fu and Y. D. Li, *Appl. Catal. B: Environ.* , 2014, **148-149**, 36.
51 Y. Z. Li, B. L. Xu, Y. N. Fan, N. Y. Feng, A. D. Qiu, J. W. M. J. He, H. P. Yang and Y. Chen, *J. Mol. Catal. A: Chem.*, 2004, **216**, 107.
52 F. B. Zhang, M. Li, L. Yang, S. Z. Ye and L. H. Huang, *Catal. Commun.* , 2014, **43**, 6.
53 M. C. Biesingera, L. W. M. Lau, A. R. Gerson and R. St. C. Smart, *Appl. Surf. Sci.*, 2010, **257**, 887.
54 W. G. Augustyna, R. I. McCrindle and N. J. Coville, *Appl. Catal. A: Gen.*, 2010, **388**, 1.
55 A. Pachulski, R. Schödel and P. Claus, *Appl. Catal. A: Gen.*, 2011, **400**, 14.
56 E. López, S. Ordóñez and F. V. Díez, *Appl. Catal. B: Environ.* , 2006, **62**, 57.
57 Y. Azizi, C. Petit and V. Pitchon, *J. Catal.*, 2008, **256**, 338.

